IEEE Access
Multidisciplinary | Rapid Review | Open Access Journal

Received April 15, 2019, accepted May 6, 2019, date of publication May 9, 2019, date of current version May 22, 2019.

Digital Object Identifier 10.1109/ACCESS.2019.2915915

Numerical Study on the Relationship Between the Localized Depression Erosion of a Commercial Blast Furnace Hearth Lining and the Heat Flux of Cooling Staves

YANG LI, (Member, IEEE), LIANGYU CHEN, AND JIAOCHENG MA
School of Mechanical Engineering and Automation, Northeastern University, Shenyang 110819, China

Corresponding author: Liangyu Chen (clysd@sina.com)

This work was supported in part by the Fundamental Research Funds for the Central Universities under Grant N180304020.

ABSTRACT The service life of a blast furnace hearth is considered as a key factor limiting the service life of a blast furnace. The erosion of the hearth lining is generally inhomogeneous, and localized depression erosion often occurs. Since the conditions inside the blast furnace hearth cannot be directly measured, it is a common practice to use the existing thermal parameters to estimate the erosion, which can provide a basis for the safe production of the blast furnace. In this context, based on the anatomical data of the No. 2 commercial blast furnace, the three-dimensional erosion model is established, and the feasibility of the computational model is verified. Then, 15 computational models with localized depression erosion at different locations are established. The finite element method is used to simulate the heat flux of the cooling staves of each model. The results show that under normal cooling and heat transfer conditions, the remaining thickness of the hearth lining is inversely proportional to the heat flux of the cooling staves. The closer the localized depression erosion is to the cooling stave, the greater the effect on the heat flux of the cooling stave. If the localized depression erosion is far enough away from the cooling stave, it will have little effect on the heat flux of the cooling stave. On this basis, we summarized a method of judging the location of localized depression erosion according to the relationship between the localized depression erosion and the cooling stave heat flux. It should be noted that when the localized depression erosion is located at the junction of the cooling staves, the increase in heat flux will not be too large, which is easily overlooked. In order to prevent the occurrence of safety accidents, we should pay more attention to this situation.

INDEX TERMS Blast furnace, cooling stave, finite element methods, heat flux, localized depression, simulation.

I. INTRODUCTION

The service life of a modern blast furnace is mainly determined by the remaining thickness of the hearth lining [1]–[5]. Safety is considered as the most significant issue for the blast furnace operation. The hearth is the most accident-prone part, and once the hearth accident will cause huge safety risks and economic losses. Caused by hot metal scouring, thermal stress, and chemical erosion, etc., the remaining thickness of the hearth lining reduces constantly [1], [6]–[9]. Since the erosion of the hearth lining is caused by a variety of complicated factors, the erosion is often inhomogeneous, and sometimes serious localized depression erosion may occur.

If the inhomogeneous erosion is not treated in time, the service time of the blast furnace will be greatly shortened. On September 1, 2017, the New No.1 blast furnace of Benxi Ironmaking Plant was burned through, causing a massive fire [10]. On August 25, 2014, the New No.3 blast furnace in a steel plant was burned through, causing a fire and one death [11]. On October 27, 2012, a 1780m^3 blast furnace was burned through, with a service life of only 3 years and 10 months [12]. On February 5, 2012, a 2800m^3 blast furnace in Tianjin Tiantie Metallurgy Group was burned through, with a service life of only 2 years and 7 months [13]. On August 20, 2010, the No.1 blast furnace of Shagang

The associate editor coordinating the review of this manuscript and approving it for publication was Bora Onat.

Group was burned through, causing a fire [11]. Investigations on the above-mentioned blast furnaces show that there is serious inhomogeneous erosion in their hearths. It is precisely because the serious inhomogeneous erosion of hearth was not found in time that the above-mentioned safety accidents were caused. We believe that the root cause is the lack of a correct understanding of the heat transfer process in the furnace.

To extend the service life of the blast furnace, it is necessary to carry out furnace protection operation when hearth localized depression erosion occurs [5], [14]. Common protective measures include limiting production, adding titanium ore [15], [16], and strengthening cooling intensity [17]. Mastering the location of the localized depression erosion can make the furnace protection work more targeted. However, due to the high temperature inside the hearth, it is difficult to observe localized depression erosion directly. Therefore, it is especially important to investigate how to use existing thermal measurement parameters to judge the location of localized depression erosion.

During the construction of a blast furnace, some thermocouples will be placed in the hearth lining according to certain rules. Many researches have focused on how to take advantage of the data measured by thermocouples to estimate the location of localized depression erosion. And many achievements have been made [18]–[23]. In the case of a sufficiently effective thermocouples, the erosion profile of the hearth can be predicted relatively accurately. However, all these works are built on the condition where there are enough effective thermocouples. Because of a long-term working under high temperature, some thermocouples are invalidated at the later period of blast furnace service. If there are too many invalidated thermocouples, the above methods will no longer be applicable.

In addition to thermocouple data, the cooling stave heat flux also can be used to judge the location of localized depression erosion. However, most of the studies on localized depression erosion are related to thermocouples, and few are related to the heat flux of cooling stave. After a large number of thermocouples are invalidated, we will have to rely on the heat flux of the cooling stave to ensure safe production. Therefore, it is necessary to carry out related study on the regularity of localized depression erosion and cooling stave heat flux.

In December 2013, the No. 2 blast furnace of a steel plant was overhauled due to the abnormal increase of cooling stave heat load. By dissecting the blast furnace, it was found that the hearth lining corresponded to the abnormal heat load area of the cooling staves had serious localized depression erosion, and the remaining thickness of the lining in the thinnest part was 315 mm. Taking this blast furnace as an example, related research was conducted. In this article, our main objectives are: (1) to construct an erosion computational model based on the measured erosion morphology of the No. 2 blast furnace hearth. Then compare the simulation results with the measured results to verify the feasibility of the computational model. (2) to construct computational models with localized depression erosion (in fifteen typical locations). And analyze the relationship between the localized depression erosion location and the cooling stave heat flux. And (3) to summarize a method of judging the location of localized depression erosion.

TABLE 1. Materials thermal conductivity [24]–[26].

Materials	λ (W/(m^2·K))
ceramic cup	4.5
micro-pore carbon brick	12.0
semi-graphite carbon brick	9.0
carbon ramming mix	9.0
cooling stave	40.0
insulating refractory mix	0.3
furnace shell	50.0

II. MODELS AND METHODS

A. PHYSICAL MODELS

The refractory materials of the No. 2 blast furnace hearth include ceramic cup, micro-pore carbon brick and semi-graphite carbon brick. Its design structure is illustrated in Fig. 1(a). The thickness of carbon ramming mix between the cooling stave and the lining is 100mm, the thickness of cooling stave is 120mm, the thickness of insulating refractory mix between the cooling stave and the furnace shell is 40mm, and the thickness of the furnace shell is 40mm.

There are three segments of cooling staves in the hearth region. Each segment has 32 cooling staves evenly distributed in the circumferential direction. There are gaps between different cooling staves. The gap between the different segments of the cooling staves is 67.5mm, and that between the same segments of the cooling staves is 50mm. The gaps are filled with carbon ramming mix. The cooling staves of each segment are arranged alternately, as shown in Fig. 1(b). Note: Only a portion of the cooling staves are shown in the figure.

The cooling water pipe in the cooling stave is a serpentine pipe with an inner diameter of 45mm. The center of the water pipe is distributed in the middle face of the cooling stave. The serpentine pipe is bent three times in the stave and it can be equivalent to 4 pipes. The cooling water velocity is 3m/s, the average temperature is 30°C. The thermal conductivity of the materials in the model is shown in Table 1.

Under normal operating conditions, the hot iron produced by the chemical reaction continuously flows into the hearth and flows out from the tap hole. Under the action of forced convection heat transfer of water in the cooling stave and natural convection heat transfer of air outside the shell, the heat of the hot iron inside the hearth is continuously transmitted from the inside to the outside, and is carried away by the water and the air.

B. METHODS

In this paper, the finite element method [27]–[32] is used for simulation, which is a numerical method commonly used

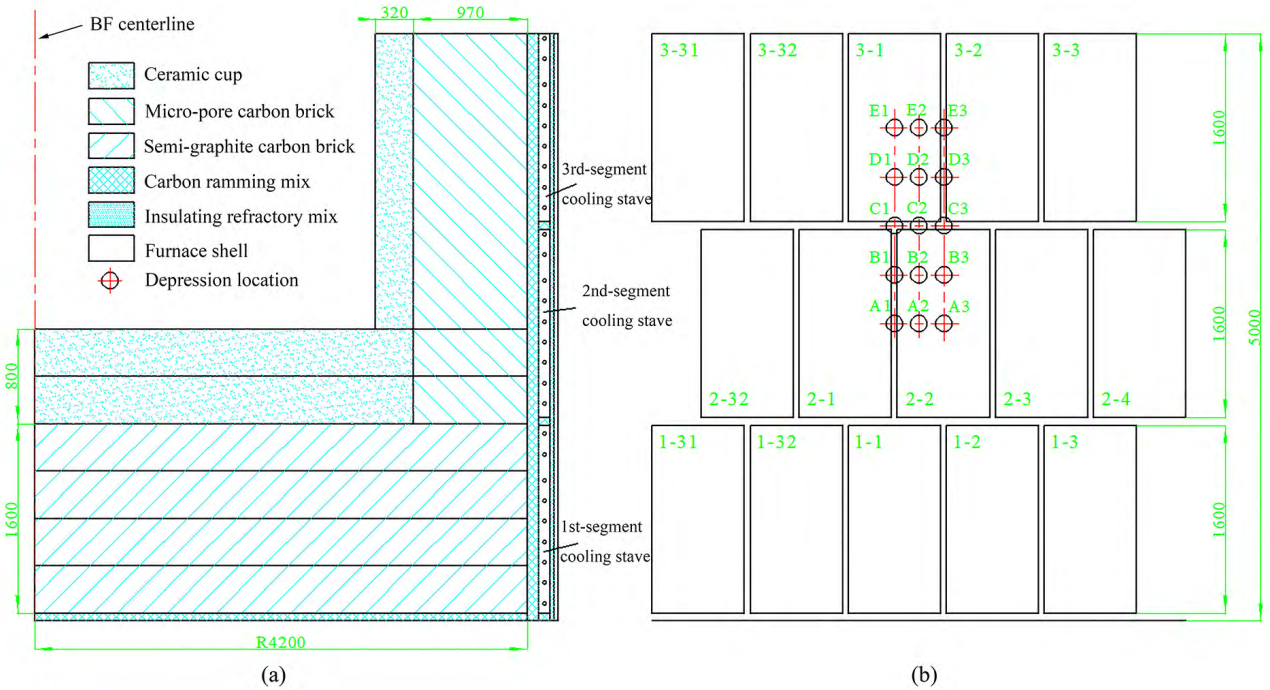

FIGURE 1. The structure diagram of the No. 2 blast furnace hearth. (a) Hearth design structure. (b) The location distribution map of the cooling staves. (size in mm).

in solving engineering problems. In the field of scientific computing, it is often necessary to solve various differential equations, and the analytical solutions of many differential equations are generally difficult to obtain. The principle of the finite element method is to discretize a differential equation into a number of simple differential equations, and then solve it with professional software. The calculation software used in this paper is ANSYS (version 19.2), which is widely used for simulating engineering problems.

1) HEAT CONDUCTION DIFFERENTIAL EQUATION

The heat transfer of the blast furnace hearth follows the law of conservation of energy. The three-dimensional unsteady heat conduction differential equation in cylindrical coordinate system [33], [34] can be described as

$$\rho c\frac{\partial t}{\partial \tau}=\frac{1}{r}\frac{\partial}{\partial r}(\lambda r\frac{\partial t}{\partial r})+\frac{1}{r^2}\frac{\partial}{\partial \varphi}(\lambda\frac{\partial t}{\partial \varphi})+\frac{\partial}{\partial z}(\lambda\frac{\partial t}{\partial z})+\dot{\mathbf{\Phi}} \quad (1)$$

where, ρ, c, λ, $\dot{\mathbf{\Phi}}$ and τ are the density, the specific heat capacity, the thermal conductivity, the heat generated per unit time by the internal heat source per unit volume, and time, respectively. And r, φ, z are the cylindrical coordinate system.

Due to the long blast furnace tapping time, the heat transfer in the blast furnace hearth is relatively stable. The heat transfer process can be regarded as a steady-state process. The transient term

$$\rho c\frac{\partial t}{\partial \tau}=0 \quad (2)$$

The direction of heat transfer is from the lining hot face to the inner surface of the cooling water pipe and the surface of the furnace shell. There is no heat source inside the model. The source term

$$\dot{\mathbf{\Phi}}=0 \quad (3)$$

Besides, the thermal conductivity of the materials is considered to be constant. Equation 1 can be simplified to the following form

$$\frac{1}{r}\frac{\partial}{\partial r}(r\frac{\partial t}{\partial r})+\frac{1}{r^2}\frac{\partial^2 t}{\partial \varphi^2}+\frac{\partial^2 t}{\partial z^2}=0 \quad (4)$$

2) EQUIVALENT CONVECTIVE HEAT TRANSFER COEFFICIENT OF HEARTH BOTTOM COOLING PIPE

The convective heat transfer coefficient at the inner surface of the stave pipe can be taken according to the empirical formula [25]

$$h_{water}=208.8+47.5v_{water}\ W/(m^2\cdot K) \quad (5)$$

where, v_{water} is the cooling water speed, m/s.

The heat flow of a single water pipe at unit length is

$$\Phi_{pipe}=\pi D_{pipe}h_{water}\Delta T_m\ W \quad (6)$$

where, D_{pipe} is the inner diameter of pipe, m. ΔT_m is the mean temperature difference between the fluid and the solid surface on the heat exchanger surface, K.

According to the wetted perimeter [35] method, the equivalent convective heat transfer coefficient of the hearth bottom is calculated. It is equivalent to the convective heat transfer coefficient at the inner surface of the water pipe. The equivalent convective heat transfer coefficient of the hearth bottom

is h_{equ}. The heat flow of the hearth bottom at unit length can be expressed as

$$\Phi_{equ} = d_{hearth} h_{equ} \Delta T_m \, W \tag{7}$$

where, d_{hearth} is the diameter of the hearth.

Obtained by the law of conservation of energy

$$\Phi_{equ} = N_{pipe} \Phi_{pipe} \tag{8}$$

where, N_{pipe} is the number of cooling pipes in hearth bottom.

Obtained by equation 6, 7 and 8

$$h_{equ} = \frac{\pi N_{pipe} D_{pipe} h_{water}}{d_{hearth}} \, W/(m^2 \cdot K) \tag{9}$$

3) ASSUMPTIONS AND BOUNDARY CONDITIONS

1. Because the tap hole is far enough away from the erosion location, it is not considered in this study [26].
2. The temperature of the erosion surface is set to 1150°C (solidification temperature of carbon saturated iron) [25].
3. The convective heat transfer coefficient on the inner surface of the cooling stave pipe is calculated by (5). It is calculated to be 351.3W/(m^2·K). Apply it to the inner surface of water pipe, and the ambient temperature is 30°C.
4. Equivalent convective heat transfer coefficient of hearth bottom is calculated by (9). It is calculated to be 50W/(m^2·K), and the ambient temperature is 30°C.
5. The furnace shell is in a natural convection environment. The convective heat transfer coefficient is taken as 10W/(m^2·K), and the ambient temperature is 30°C [26].
6. Only a part of the hearth is selected for simulation calculation. It is assumed that there is no heat conduction between this part and its adjacent part, and thus the contact face is set to heat insulating surface. The feasibility analysis of model simplification is presented in section C 2).

C. COMPUTATIONAL DOMAIN SELECTION AND MODEL EVALUATION

During the anatomical study of the blast furnace, it was found that the hearth lining corresponded to the abnormal heat load area of the cooling staves had serious localized depression erosion, and the remaining thickness of the lining in the thinnest part was 315mm (Fig. 2). The positional relationship between the localized depression erosion and the cooling staves is shown in Fig. 3. According to the measured erosion morphology, the computational models of this region is constructed.

In order to save the calculation cost, only a part of the hearth is taken for calculation. In this paper, only the relationship between the localized depression erosion and the heat flux of the cooling staves nearby is concerned. If the selected computation area is large enough (the cutoff boundary is far enough away from the depression area), the effect of the cutoff boundary on the heat flux of the cooling staves near the localized depression can be negligible. However, under the same calculation accuracy, the large computation area will increase the computation cost. While ensuring the accuracy of the simulation calculation, the calculation domain should be reduced as much as possible.

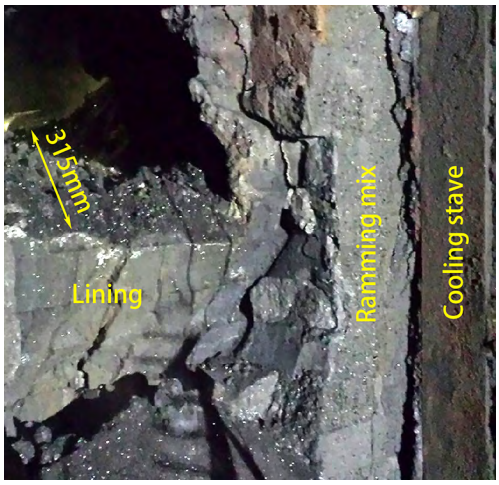

FIGURE 2. Anatomical image of localized depression erosion of the No.2 blast furnace hearth.

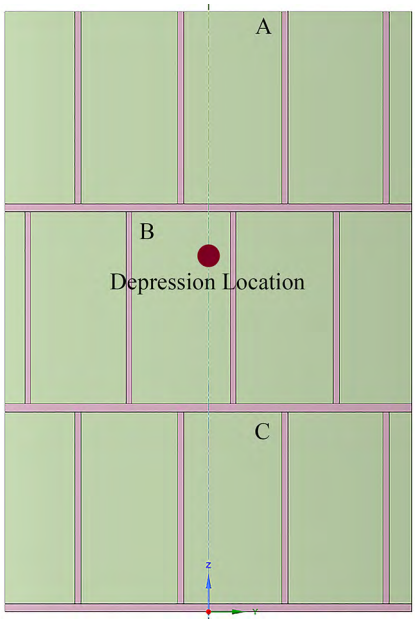

FIGURE 3. Positional relationship between the localized depression erosion and cooling staves.

As shown in Fig. 4, the hearth regions corresponding to the number of cooling staves of 2.0, 2.5, 3.0, 3.5, and 4.0 in the circumferential direction were respectively selected as computational model. All models are centered on the localized depression erosion.

1) MESHING AND MESH INDEPENDENCE VERIFICATION

In finite element analysis, the model needs to be discretized into a mesh model. In general, the denser the meshes,

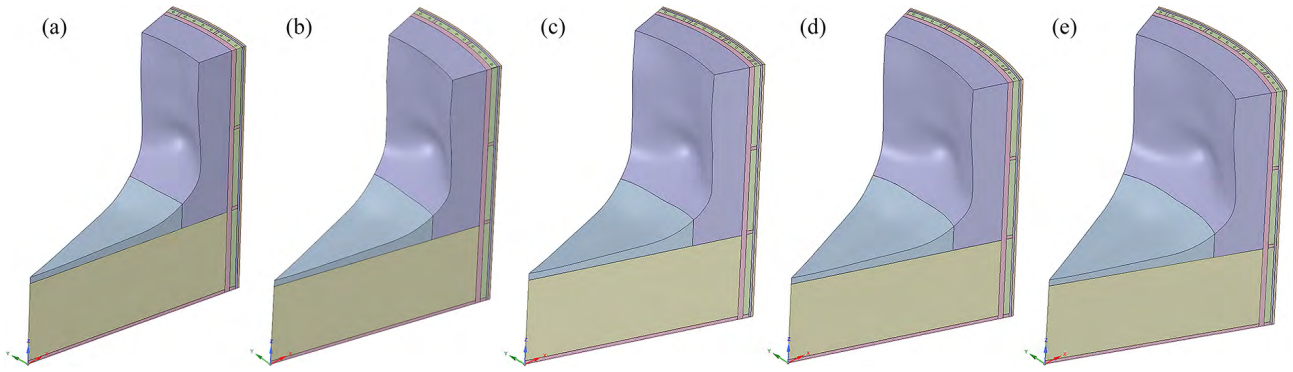

FIGURE 4. Computational models with different size computational domains (Classified by the number of cooling staves in the circumferential direction). (a) 2.0 cooling staves; (b) 2.5 cooling staves; (c) 3.0 cooling staves; (d) 3.5 cooling staves; (e) 4.0 cooling staves 0.

FIGURE 5. Mesh of the model with 3.5 cooling staves.

the higher the accuracy of the solution, but the cost of the solution will also increase. Taking the model with 3.5 cooling staves as an example, the mesh independence analysis is developed.

The cooling staves are discretized by encrypted hexahedral meshes. The rest of the model are discretized by looser tetrahedral meshes. Fig. 5 is the meshes of the model. There are about 3.298×10^6 meshes in the model. The density of the mesh will influence the calculation results. The simulation calculation is performed for the model with mesh numbers of 3.298×10^6, 4.646×10^6, 6.060×10^6 and 8.318×10^6. The heat flux of the cooling staves code A, B, and C are used to evaluate the density of the mesh on the calculation results. (Cooling staves code is shown in Fig. 3.) The results are shown in Table 2.

TABLE 2. The heat flux of cooling staves (kw/m^2).

Mesh number	Stave A	Stave B	Stave C
3.298×10^6	4.778	21.024	21.819
4.646×10^6	4.775	21.008	21.827
6.060×10^6	4.772	21.018	21.841
8.318×10^6	4.777	21.037	21.855

The above four mesh numbers have little effect on the heat flux of the cooling staves A, B and C. It means the model with 3.298×10^6 meshes can meet the accuracy requirement. The mesh density is used in all the models in this paper.

2) CUTOFF BOUNDARY INDEPENDENCE VERIFICATION

The five models in Fig. 4 are meshed and simulated. Fig. 6 shows the heat flux fields of the three of these models. It can be observed that when the cutoff boundary changes, the heat flux distribution of the hearth lining is basically the same. The heat flux in the depression area is significantly larger than that in other areas. These phenomena are in line with physical laws.

The heat flux of the cooling staves code A, B, and C are used to evaluate the effect of the cutoff boundary on the calculation results. The average heat flux of the three cooling staves are extracted, as shown in Fig. 7. It can be observed that as the number of circumferential cooling staves increases (the cutoff boundary becomes farther from the depression area), the heat flux values of the respective cooling staves tend to be stable. Compared with the model with 3.5 cooling staves in the circumferential direction, when the number of staves is 4.0, the difference percentages of heat flux values of cooling staves A, B, and C are 0.32%, 0.59%, and 0.86%, respectively, which can meet the needs of engineering calculation accuracy. When the number of cooling staves is from 3.5 to 4.0, the calculation accuracy increases slightly, but the amount of calculation increases substantially. Therefore, in this study, the model with 3.5 cooling staves in circumferential direction is selected for calculation. Its temperature

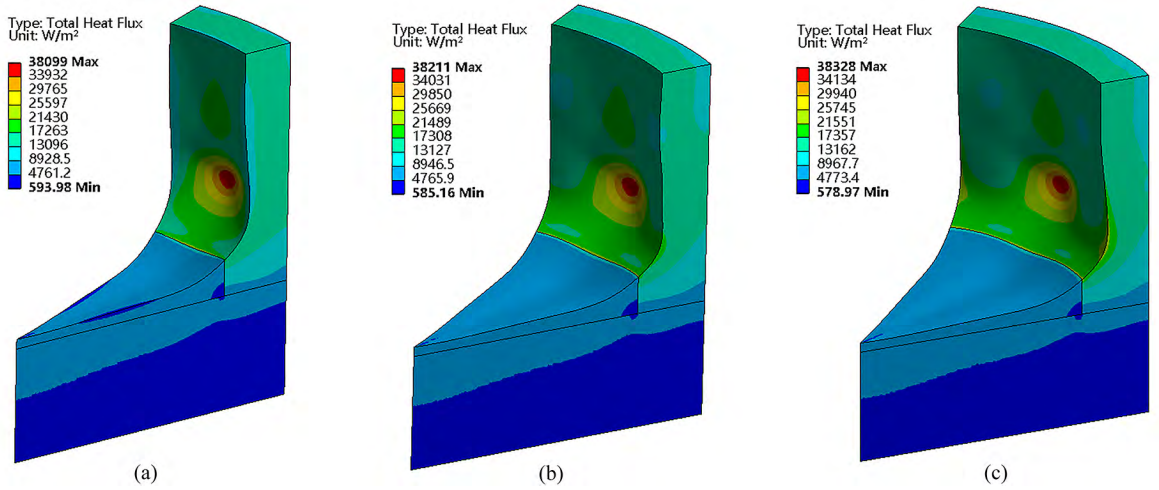

FIGURE 6. Heat flux field of the hearth lining. (a) 2.0 cooling staves; (b) 3.0 cooling staves; (c) 4.0 cooling staves.

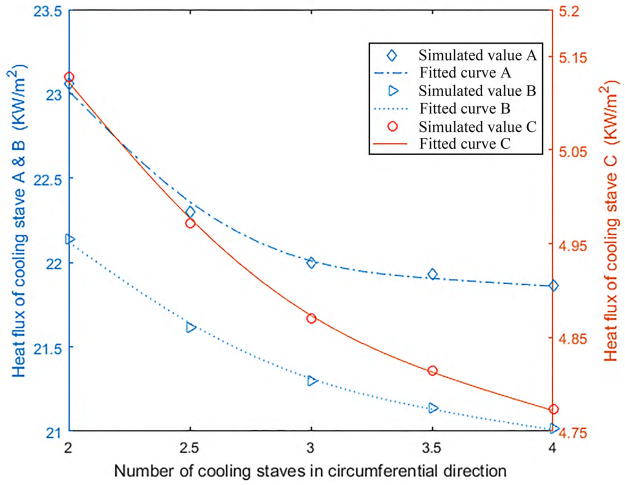

FIGURE 7. The simulation values of the heat flux of the cooling staves code A, B, and C, obtained by different computational models.

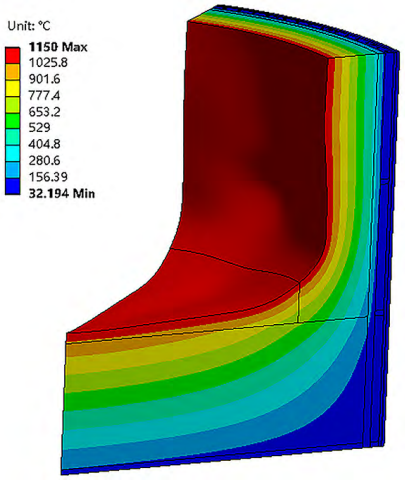

FIGURE 8. The simulated temperature field of the model with 3.5 cooling staves in the circumferential direction.

field is shown in Fig. 8. The temperature of the hearth gradually decreases from the inside out, which is consistent with the real situation.

Fig. 9 shows the measured and simulated heat flux values of the cooling staves code A, B, and C. The simulated values are in good agreement with the measured values. Therefore, the results of the simulation calculations are reliable.

D. THREE-DIMENSIONAL COMPUTATIONAL MODELS WITH LOCALIZED DEPRESSION EROSION

To study the relationship between the location of localized depression erosion and the heat flux of cooling stave, the computational model needs to accurately describe the positional relationship between them. When constructing models, the shape of the depression should be as consistent as possible.

Anatomical study shows that the erosion in the northwest direction of the hearth is relatively uniform. The base model (Fig. 10(a)) is established according to the erosion in this direction. Localized depression erosion may occur in the corresponding area of a single stave, at the junction of two or three staves, or between them. The typical locations are shown in Fig. 1(b).

The computational models are constructed by cutting the base model with a ball (radius 500mm). Ensure that the center of the ball is 900mm from the outside of the lining, that is, the thinnest remaining thickness of the lining is 400mm. The constructed three-dimensional models A1-E1 are shown in Fig. 10(b-f). Compared with them, models A2-E2, A3-E3 (not shown separately) are differ in the location of the cooling staves.

III. RESULTS AND DISCUSSION

A. RELATIONSHIP BETWEEN THE LOCALIZED DEPRESSION EROSION AND THE HEAT FLUX OF COOLING STAVES

Fig. 11 and Fig. 12 show the temperature fields and the heat flux fields of the middle section of the base model, model

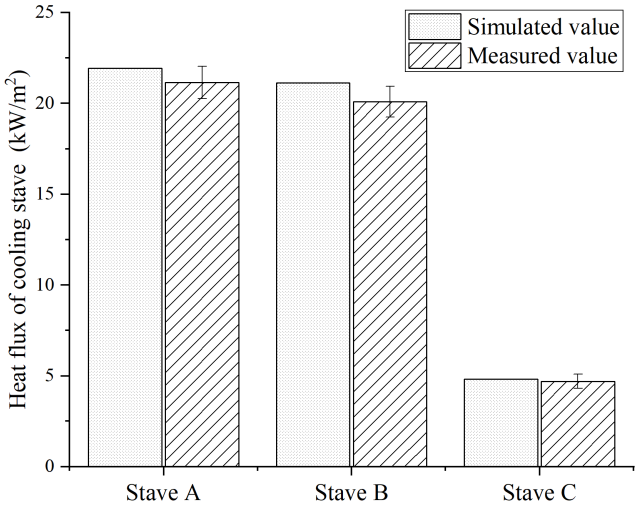

FIGURE 9. The simulated and measured heat flux of the cooling staves A, B, and C.

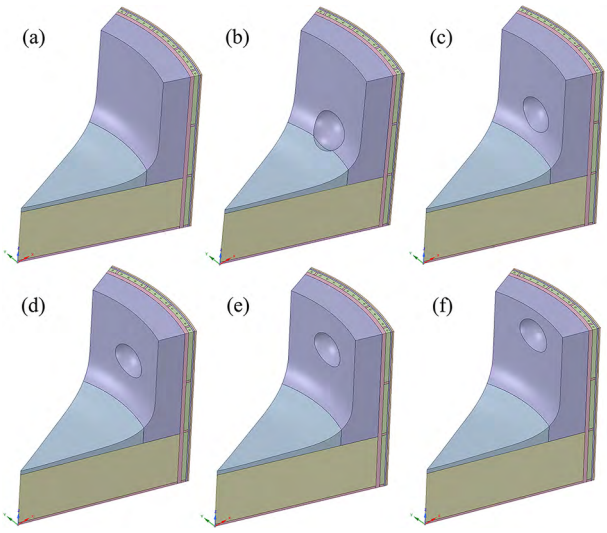

FIGURE 10. Three-dimensional computational models. (a) Base model; (b) Model A1; (c) Model B1; (d) Model C1; (e) Model D1; (f) Model E1.

A1, and model C1, respectively. As shown in Fig. 11, the temperature of the lining is high inside and low outside, that is, the direction of heat transfer in the lining is from the inside to the outside. As shown in Fig. 12, the heat flux at the localized depression is significantly higher than that at other locations. The maximum heat flux of the base model is 28372W/m^2, while the model A1 and model C1 are 36559W/m^2 and 34558W/m^2, respectively. Their difference is 28.9% and 21.8% respectively. Under the normal cooling and heat transfer conditions, the remaining thickness of the hearth lining is inversely proportional to the heat flux. This is due to the decrease of thermal resistance of lining caused by localized depression erosion, which increases the heat transferred from the depression area in unit time.

Since the cooling stave is located inside the furnace shell, only the average heat flux of the monolithic stave can be measured by existing measurement techniques. Therefore, the simulated average heat flux value of each cooling stave is extracted for study, as shown in Table 3. The relationships between localized depression erosion and cooling stave average heat flux are discussed below. The conclusions are drawn from the comparison with the base model.

TABLE 3. Average simulated heat flux of cooling staves (W/m^2).

Stave code	Base model	Model A1	Model B1	Model C1	Model D1	Model E1
1-1	4392	5140	4512	4432	4417	4414
1-2	4394	4900	4476	4420	4409	4406
2-1	16475	19710	18539	17677	17014	16711
2-2	16471	19605	18439	17582	16924	16622
3-1	19797	20002	20368	21176	21988	22358
3-2	19803	19925	20068	20352	20639	20789
		Model A2	Model B2	Model C2	Model D2	Model E2
1-1	-	5116	4505	4427	4413	4409
1-2	-	4969	4480	4415	4403	4400
2-1	-	18926	17957	17316	16832	16601
2-2	-	20163	18847	17813	17010	16651
3-1	-	20010	20357	21116	21881	22232
3-2	-	20032	20240	20671	21107	21320
		Model A3	Model B3	Model C3	Model D3	Model E3
1-1	-	4805	4500	4428	4414	4411
1-2	-	4793	4490	4417	4404	4401
2-1	-	18156	17467	17040	16730	16573
2-2	-	20299	18980	17875	17013	16630
3-1	-	20021	20349	20963	21583	21875
3-2	-	19962	20290	20905	21525	21816

According to the data in Table 3, it is not difficult to find that localized depression erosion can increase the heat flux of the cooling staves nearby. The closer the localized depression erosion is to the cooling stave, the greater the effect on the heat flux of the cooling stave. It is caused by the large amount of heat transferred from the localized recessed location.

Define the percentage difference from base model is

$$\delta = \frac{q_d - q_b}{q_b} \times 100\% \tag{10}$$

where, q_d is the cooling stave heat flux of the models with localized depression erosion, W/m^2. q_b is the cooling stave heat flux of the base model, W/m^2.

The percentage difference of the computational models A1-E1 is shown in Fig. 13(a). The percentage difference of the computational models A2-E2 is shown in Fig. 13(b). And the percentage difference of the computational models A3-E3 is shown in Fig. 13(c).

Model A1, model A2 and model A3 are taken as examples for discussion. The heights of the localized depression erosion of these three models are the same. In model A1, the deepest location of the depression erosion corresponds to the junction of the cooling stave 2-1 and cooling stave 2-2. The percentage difference of the cooling stave 2-1 and cooling stave 2-2 are 19.6% and 19.0%, respectively. In model A3, the deepest location of the depression erosion corresponds to the center of the cooling stave 2-2. The percentage difference of the cooling stave 2-1 and cooling stave 2-2 are 10.2% and

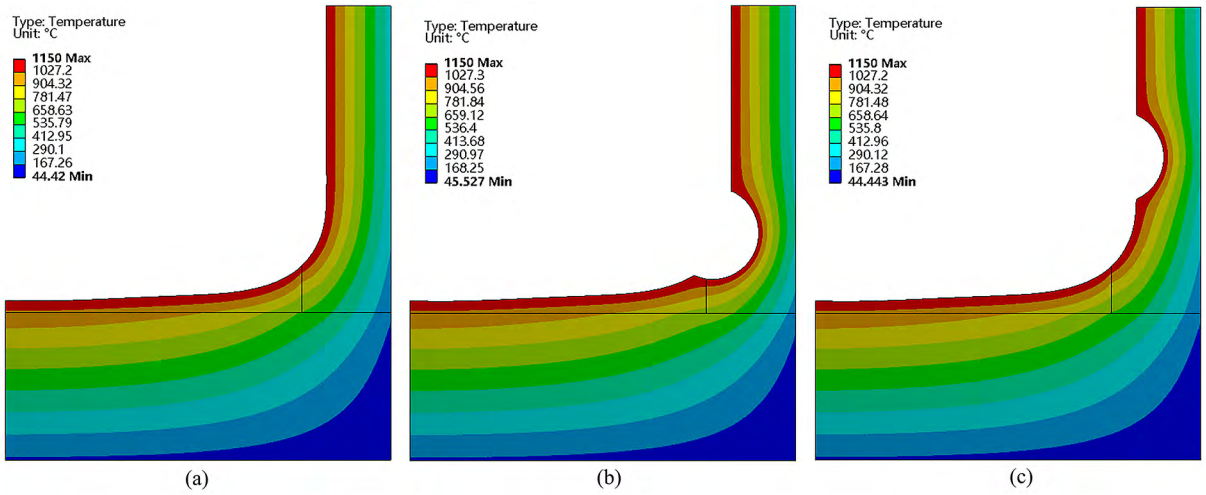

FIGURE 11. Temperature fields of the hearth lining middle section. (a) Base model; (b) Model A1; (c) Model C1.

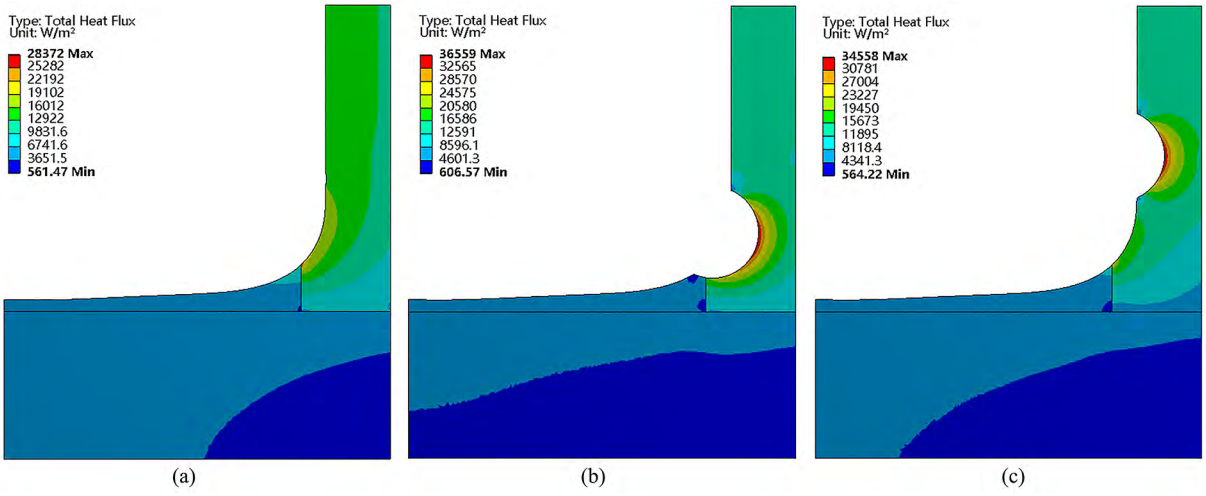

FIGURE 12. Heat flux fields of the hearth lining middle section. (a) Base model; (b) Model A1; (c) Model C1.

23.2%, respectively. In model A2, the deepest location of the depression erosion is located in the middle of the depression location of model A1 and model A3. The percentage difference of the cooling stave 2-1 and cooling stave 2-2 are 14.9% and 22.4%, respectively. It is found that the heat flux value of cooling stave is sensitive to the localized depression erosion when the depression corresponds to a single cooling stave. As the localized depression erosion deviates to the boundary of the cooling stave, the sensitivity of the cooling stave heat flux to the depression is gradually reduced.

In contrast to model A3, model B3, model C3, model D3, and model E3, the height of localized depression erosion is increasing. The localized depression erosion gradually moves away from the 1st-segment (1-1, 1-2) and the 2nd-segment (2-1, 2-2) cooling stave, and gradually approaches the 3rd-segment (3-1, 3-2) cooling stave. As shown in Fig. 13 (c), the percentage difference of the 1st-segment and 2nd-segment cooling stave is continuously decreasing, while the percentage difference of the 3rd-segment cooling stave is increasing. This confirms the previous conclusion: the closer the localized depression erosion is to the cooling stave, the greater the effect on the heat flux of the cooling stave. When the location of the localized depression erosion is transferred from D3 to E3, the heat flux of the 1st-segment cooling staves changes very little. It shows that if the localized depression erosion is far enough away from the cooling stave, it will have little effect on its heat flux.

In model C3, the deepest location of the localized depression erosion corresponds to the junction of the cooling stave 2-2, cooling stave 3-1 and cooling stave 3-2. The percentage difference of all six cooling staves is less than 10% (2-2 cooling stave is the largest, 8.5%). The change of heat flux of each cooling stave is relatively small. It is because the total heat transferred from the eroded location is constant.

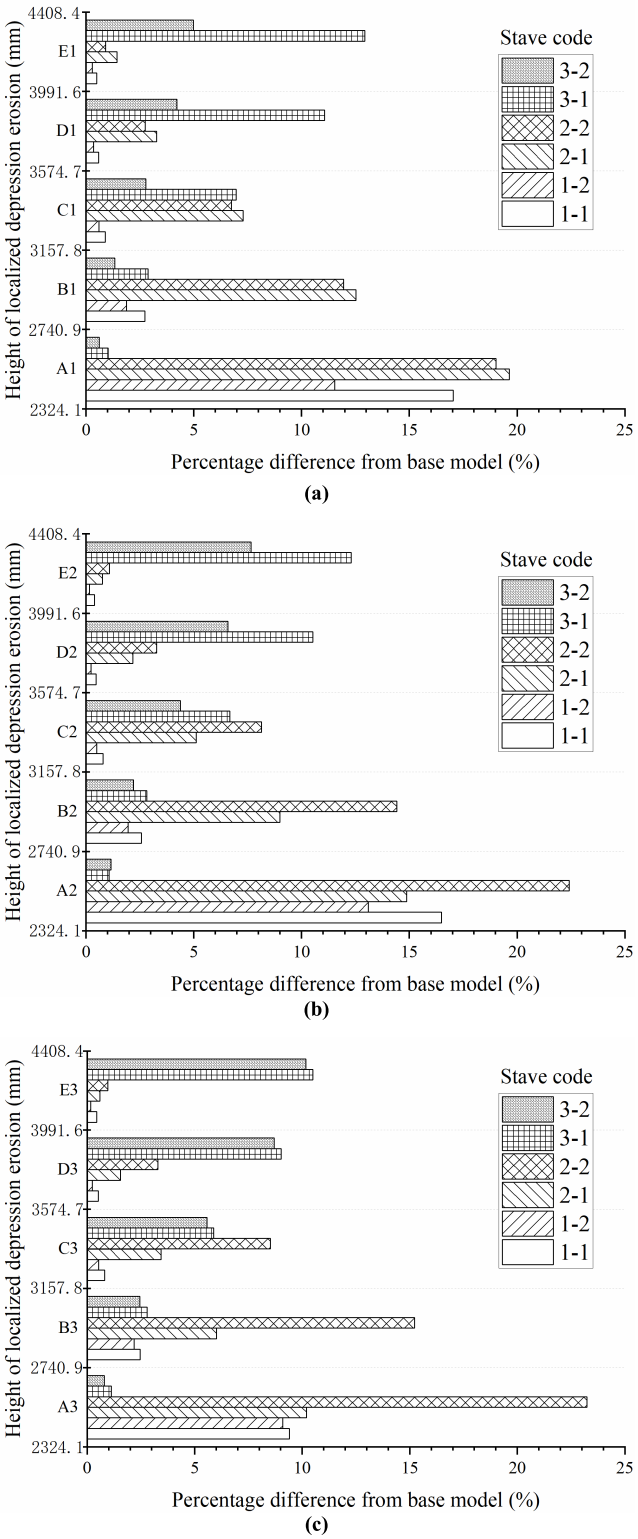

FIGURE 13. Percentage difference of cooling staves heat flux between the computational models with localized depression erosion and the base model. (a) Model A1-E1; (b) Model A2-E2; (c) Model A3-E3.

When the localized depression erosion occurs at their junction, the increased heat is shared by them. This situation is very easy to be ignored by blast furnace operators. However, the junction of cooling stave is a weak cooling area, which is prone to localized depression erosion. In order to ensure the safe production of the blast furnace, we need to maintain sufficient vigilance against this situation.

B. JUDGING THE LOCATION OF LOCALIZED DEPRESSION EROSION BASED ON COOLING STAVE HEAT FLUX

The location of the localized depression erosion can be judged according to the relationship between the localized depression erosion and the cooling stave heat flux. If localized depression erosion occurs, the heat flux of cooling staves near the depression will definitely increase. When judging the location of localized depression erosion, we should not only consider the heat flux of the cooling stave with the highest heat flux, but also the heat flux of all the cooling staves adjacent to it. In actual production, there is no basic model. Usually, the average heat flux of the cooling staves in the same segment can be referred to. To judging the location of the localized depression erosion, we should obtain the heat flux of the abnormal cooling stave and the surrounding cooling staves firstly. Then, calculate their percentage difference. Finally, compare with the fifteen cases in Fig. 13 and find the most similar case. The location of the actual localized depression erosion should be located near the erosion location of the case.

The location of localized depression erosion can be roughly divided into the following cases:

1. If the increase in the heat flux of a certain cooling stave is significant, and the increase of the cooling staves adjacent to it is small, the localized depression erosion may occur in the corresponding area of the cooling stave. The greater the difference between them, the closer the localized depression erosion is to the center of the cooling stave.
2. If the heat flux of two adjacent cooling staves in the same segment increases simultaneously, and there is no abnormality in the adjacent staves, the localized depression erosion may occur in the corresponding area of their junction. If the increase in the heat flux of the two cooling staves is different, the location of the localized depression erosion is biased toward the larger one.
3. If the heat flux of two or three adjacent cooling staves in two adjacent segments increases at the same time, the localized depression erosion may occur in the corresponding area of their junction.

If conditions permit, the furnace shell temperature in this area should be measured as an additional judgment parameter. If the shell temperature is abnormal too, it can be verified that there is localized depression erosion in this area. As mentioned above, when localized depression corresponds to the junction of multiple cooling staves, the increase in heat flux is not significant. Therefore, when Case 2 and Case 3 conditions occur, we recommend measuring the shell temperature for verification.

IV. CONCLUSION

Taking the No. 2 blast furnace as the research object, we discussed the variation of the heat flux of the cooling staves when the localized eroded erosion location (in fifteen typical locations) changes. We found that under normal cooling and heat transfer conditions, the remaining thickness of the hearth lining is inversely proportional to the heat flux of the cooling staves. The closer the localized depression erosion is to the cooling stave, the greater the effect on the heat flux of the cooling stave.

We also found that when the localized depression erosion corresponds to a single cooling stave, the heat flux increases relatively large. However, when the localized depression erosion corresponds to the junction of the stave, the increase in the heat flux is relatively small. In blast furnace safety monitoring, the safe value of the stave heat flux is often set to a fixed value, which causes frequent burning through accidents of the hearth. We should pay enough attention to it.

After the localized depression erosion of the hearth occurs, the furnace protection work should be carried out as soon as possible to slow down the erosion rate. We summarized a method of judging the location of localized depression erosion according to the heat flux of the cooling staves, which can provide a basis for more effective measures to protect the furnace.

REFERENCES

[1] A. Shinotake, H. Ootsuka, N. Sasaki, and M. Ichida, "Blast furnace campaign life relating to the productivity," *Metall. Res. Technol.*, vol. 101, no. 3, pp. 203–209, Mar. 2004.

[2] Y. Zhang, R. Deshpande, D. Huang, P. Chaubal, and C. Q. Zhou, "Numerical analysis of blast furnace hearth inner profile by using CFD and heat transfer model for different time periods," *Int. J. Heat Mass Transf.*, vol. 51, nos. 1–2, pp. 186–197, Jan. 2008.

[3] K. Jiao, J. Zhang, Q. Hou, Z. Liu, and G. Wang, "Analysis of the relationship between productivity and hearth wall temperature of a commercial blast furnace and model prediction," *Steel Res. Int.*, vol. 88, no. 9, Sep. 2017, Art. no. 1600475.

[4] Y.-L. Li, S.-S. Cheng, P. Zhang, and S.-H. Zhou, "Sensitive influence of floating state of blast furnace deadman on molten iron flow and hearth erosion," *ISIJ Int.*, vol. 55, no. 11, pp. 2332–2341, 2015.

[5] F.-M. Zhang, "Design and operation control for long campaign life of blast furnaces," *J. Iron Steel Res. Int.*, vol. 20, no. 9, pp. 53–60, Sep. 2013.

[6] S. N. Silva *et al.*, "A methodology to investigate the wear of blast furnace hearth carbon refractory lining," *Mater. Corrosion*, vol. 64, no. 11, pp. 1032–1038, Nov. 2013.

[7] S. N. Silva *et al.*, "Wear mechanism for blast furnace hearth refractory lining," *Ironmak. Steelmak.*, vol. 32, no. 6, pp. 459–467, Dec. 2005.

[8] B. J. Monaghan, P. B. Drain, M. W. Chapman, and R. J. Nightingale, "Reactivity of coke ash on aluminosilicate blast furnace hearth refractories," *ISIJ Int.*, vol. 54, no. 4, pp. 810–819, 2014.

[9] M. Zagaria, V. Dimastromatteo, and V. Colla, "Monitoring erosion and skull profile in blast furnace hearth," *Ironmaking Steelmaking*, vol. 37, no. 3, pp. 229–234, Apr. 2010.

[10] SOHU. Beijing, China. (Sep. 2017). *From the Case of Burning Through the Hearth and the Explosion of the Blast Furnace, the Steel Furnace Blast Furnace Accident is Analyzed*. (in Chinese). [Online]. Available: http://www.sohu.com/a/190113276_743482

[11] Metallurgical House. Beijing, China. (Feb. 2017). *Warning of Two Burning-Through Accidents of Blast Furnace Hearth*. (in Chinese). [Online]. Available: http://www.gtjia.com/ld_article_show.asp?id=361971

[12] Y. Tan, Z. H. Huang, and F. Q. Gong, "Brief analysis on burning-through accident of No.3 BF hearth of Jiugang," (In Chinese). *Ironmaking*, vol. 34, no. 4, pp. 28–32, 2015.

[13] W. Xie, "Analysis and preventive measures of burning through accident of 2800 m^3 blast furnace hearth in Tiantie," (In Chinese). *Tianjin Metall.*, vol. 6, pp. 25–27, 2018.

[14] S. V. Filatov, I. F. Kurunov, Y. M. Gordon, D. N. Tikhonov, and S. N. Grachev, "Extending the campaign life of an intensively operating blast furnace," *Metallurgist*, vol. 60, nos. 9–10, pp. 905–911, Jan. 2017.

[15] K.-X. Jiao *et al.*, "Analysis of titanium distribution behaviour in vanadium-containing titanomagnetite smelting blast furnace," *Can. Metall. Quart.*, vol. 57, no. 3, pp. 274–282, Apr. 2018.

[16] K. M. Komiyama, B.-Y. Guo, H. Zughbi, P. Zulli, and A.-B. Yu, "Numerical analysis of titanium compounds in blast furnace hearth during titania addition," *Steel Res. Int.*, vol. 86, no. 6, Jun. 2015.

[17] W.-C. Chen and W.-T. Cheng, "Numerical simulation on forced convective heat transfer of titanium dioxide/water nanofluid in the cooling stave of blast furnace," *Int. Commun. Heat Mass Transf.*, vol. 71, pp. 208–215, Feb. 2016.

[18] J. Brannbacka and H. Saxen, "Model for fast computation of blast furnace hearth erosion and buildup profiles," *Ind. Eng. Chem. Res.*, vol. 47, no. 20, pp. 7793–7801, Oct. 2008.

[19] M. X. Feng, R. Chen, and Q. Li, "Development of erosion monitoring model for blast furnace hearth based on moving-boundary method," *Mater. Res. Innov.*, vol. 19, pp. 448–453, May 2015.

[20] L. Wu, H. Cheng, Y. Su, and H. Feng, "Mathematical model for on-line prediction of bottom and hearth of blast furnace by particular solution boundary element method," *Appl. Therm. Eng.*, vol. 23, no. 16, pp. 2079–2087, Nov. 2003.

[21] J. Torrkulla and H. Saxén, "Model of the state of the blast furnace hearth," *ISIJ Int.*, vol. 40, no. 5, pp. 438–447, May 2000.

[22] H. B. Zhao, S.-F. Huo, and S.-S. Cheng, "Study on the early warning mechanism for the security of blast furnace hearths," *Int. J. Minerals, Metall., Mater.*, vol. 20, no. 4, pp. 345–353, Apr. 2013.

[23] R. M. Duarte, I. Ruiz-Bustinza, D. Carrascal, L. F. Verdeja, J. Mochón, and A. Cores, "Monitoring and control of hearth refractory wear to improve blast furnace operation," *Ironmaking Steelmaking* , vol. 40, no. 5, pp. 350–359, Jul. 2013.

[24] Y. B. Wang, S. Y. Li, H. Jiang, and S. X. Lu, *Blast Furnace Masonry Technical Manual*, S. Y. Li, Ed. Beijing, China: Metallurgical Industry Press, (in Chinese), 2006.

[25] L. Yu, "Thermal state model and lining erosion identification of blast furnace hearth," (in Chinese), Ph.D. dissertation, School Mech. Eng. Automat., Northeastern Univ., Shenyang, China, 2009.

[26] X. G. Ma, "Simulation and optimization study on thermal-mechanical coupling characteristics of middle and lower structure of blast furnace under the heating and opening conditions," (in Chinese), Ph.D. dissertation, School Mech. Eng. Automat., Northeastern Univ., Shenyang, China, 2018.

[27] S. Kumar, "Heat transfer analysis and estimation of refractory wear in an iron blast furnace hearth using finite element method," *ISIJ Int.*, vol. 45, no. 8, pp. 1122–1128, 2005.

[28] A. L. de Oliveira, A. Pelizari, and A. J. S. Filho, "Finite element analysis simulation of switched reluctance motor drive," *IEEE Latin Amer. Trans.*, vol. 16, no. 7, pp. 1928–1933, Jul. 2018.

[29] Y. Li, S. Sun, and L. Zhu, "Numerical modeling and De-embedding of non-planar periodic guided-wave structures via short-open calibration in 3-D FEM algorithm," *IEEE Access*, vol. 6, pp. 67329–67337, 2018.

[30] M. Zheng, Z. Qian, Z. Zou, C. Peach, and L. Ren, "Subject-specific finite element modeling of the human shoulder complex part 2: Quantitative evaluation of the effect of rotator cuff tear propagation on glenohumeral joint stability," *IEEE Access*, vol. 7, pp. 34068–34077, 2019.

[31] Y. Zhang, W. Song, M. Karimi, C.-H. Chi, and A. Kudreyko, "Fractional autoregressive integrated moving average and finite-element modal: The forecast of tire vibration trend," *IEEE Access*, vol. 6, pp. 40137–40142, 2018.

[32] Z. Wang, J. Ma, and L. Zhang, "Finite element thermal model and simulation for a cylindrical Li-ion battery," *IEEE Access*, vol. 5, pp. 15372–15379, Jul. 2017.

[33] J. P. Holman, *Heat Transfer*. New York, NY, USA: Raghothaman Srinivasan, 2010.

[34] T. Wenquan, *Numerical Heat Transfer*. Xi'an, China: Xi'an Jiao Tong Univ. press, (in Chinese), 2001, pp. 86–98.

[35] F. M. White, *Fluid Mechanics*. 2nd ed., M. Lange, Ed. New York, NY, USA: McGraw-Hill, 2009.

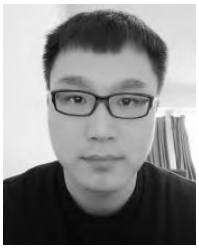

YANG LI (M'18) was born in Jinzhong, Shanxi, China, in 1991. He received the B.Eng. degree in mechanical engineering from Northeastern University, Shenyang, China, in 2014, where he is currently pursuing the Ph.D. degree in mechanical engineering.

His research interests include the safety evaluation of blast furnace hearth structure and abnormal erosion control of blast furnace hearth.

LIANGYU CHEN was born in Weifang, Shandong, China, in 1959. He received the B.Eng. degree in mechanical engineering from the China University of Petroleum, Dongying, China, in 1982, and the M.Eng. and Ph.D. degrees in mechanical engineering from Northeastern University, Shenyang, China, in 1986 and 1994, respectively.

Since 1997, he has been a Professor with the School of Mechanical Engineering and Automation, Northeastern University. He has authored 12 books and more than 80 articles. His research interests include structural integrity of metallurgical equipment, mechanical power transmission and transmission technology, and engineering equipment modeling and digital technology.

JIAOCHENG MA was born in Shanxi, China, in 1979. He received the B.Eng. and M.Eng. degrees in mechanical engineering and the Ph.D. degree in detection technology and automation device from Northeastern University, Shenyang, China, in 2002, 2005, and 2009, respectively.

He is currently an Associate Professor with the School of Mechanical Engineering and Automation, Northeastern University. He has authored more than 20 articles. His research interests include embedded design, virtual instrument development, and complex process parameter detection, modeling, and optimization control.